frontiers | Frontiers in Astronomy and Space Sciences

TYPE Original Research
PUBLISHED 21 May 2024
DOI 10.3389/fspas.2024.1291847

OPEN ACCESS

EDITED BY
Jennifer Claire Stern,
National Aeronautics and Space Administration, United States

REVIEWED BY
Svetlana Shkolyar,
University of Maryland, United States
Ashley Murphy,
Planetary Science Institute, United States

*CORRESPONDENCE
Wei Lin,
weilin@mail.iggcas.ac.cn

RECEIVED 10 September 2023
ACCEPTED 01 May 2024
PUBLISHED 21 May 2024

CITATION
Chen Y, Yin Z and Lin W (2024), Taphonomy of biosignatures in carbonate nodules from the Mars-analog Qaidam Basin: constraints from microscopic, spectroscopic, and geochemical analyses.
Front. Astron. Space Sci. 11:1291847.
doi: 10.3389/fspas.2024.1291847

Taphonomy of biosignatures in carbonate nodules from the Mars-analog Qaidam Basin: constraints from microscopic, spectroscopic, and geochemical analyses

Yan Chen[1], Zongjun Yin[2] and Wei Lin[1]*

[1]Key Laboratory of Earth and Planetary Physics, Institute of Geology and Geophysics, Chinese Academy of Sciences, Beijing, China, [2]State Key Laboratory of Palaeobiology and Stratigraphy, Nanjing Institute of Geology and Palaeontology, Chinese Academy of Sciences, Nanjing, China

Early diagenetic nodules with low permeable and weather-resistant structures are considered to be favorable for biosignature preservation. Numerous nodular structures forming in neutral-to-alkaline and saline diagenetic fluids were previously identified at Gale Crater on Mars, yet their astrobiological significance remains poorly understood. In the Mars-like western Qaidam Basin, China, there are a multitude of carbonate nodules which can be analogous to those found at Gale Crater on Mars in terms of their formation backgrounds and post-depositional processes. In this study, we combine microscopic, spectroscopic, and geochemical methods to characterize the biosignature preservation of the Qaidam nodules. Carbonaceous materials, including an organic annulus inferred to be a fossil spore or algal filament microfossil, are observed in the Qaidam nodules. The total organic carbon contents of the Qaidam nodules are slightly higher than those of the surrounding fluvio-lacustrine deposits, suggesting that early diagenesis of the Qaidam nodules might facilitate the rapid entombment of biomass within magnesium carbonate or aragonite matrixes before complete degradation. The carbonate matrix showing alternating micritic and sparry layers as well as enrichment of ^{13}C could have a physicochemical origin though the possibilities of biomineralization and organomineralization cannot be entirely ruled out. The I-1350/1,600 distribution of carbonaceous materials implies the existence of carbon precursors of various subcellular components or coexisting organisms in pore waters. Organic carbon isotopes indicate the carbon fixation pathways such as the Calvin cycle or the Wood-Ljungdahl pathway utilized by organisms in pore waters. The findings of this study shed light into the taphonomy and detection of biosignatures in terrestrial playa nodules, with potential applications for biosignature exploration on Mars.

KEYWORDS

carbonate nodules, Qaidam Basin, Mars analog, biosignatures, taphonomy

1 Introduction

Ancient Mars three to four billion years ago could have been wetter and more habitable than modern Mars. It experienced an aridification during the Noachian-Hesperian transition (Ehlmann and Edwards, 2014; Bishop, 2018). As such, rovers have been launched to the extinct aqueous-altered landforms on Mars to search for potential biosignatures. Curiosity rover landed on remnants of an ancient lakebed at Gale Crater and unveiled unexpected detailed insights into the aqueous and climatic history of early Mars (Grotzinger et al., 2012). Perseverance rover landed at Jezero Crater, once an ancient delta-lake system. The rover mission had a goal of searching for signs of life and has since collected samples cached for a follow-on return mission to Earth (Farley et al., 2020). Tianwen-1 landed on southern Utopia Planitia near suspected shorelines and had the goal of investigating the characteristics and evolution of the ancient Mars environment (Liu et al., 2021). In the NASA Mars Sample Return campaign, samples collected in early records of Mars would be returned to Earth for a thorough examination of biosignatures in sophisticated laboratories (Haltigin et al., 2022; Kminek et al., 2022). This approach is to confirm whether life exists or existed where and when environmental conditions permitted on Mars (Farley et al., 2020; Meyer et al., 2022; Simon et al., 2023). China has also planned for a sample return task in the upcoming Tianwen-3 mission around 2030 to search for evidence of life (Xu et al., 2022).

Selecting the most promising landing sites and astrobiologically relevant samples is important for the fulfillment of the Mars Sample Return Campaign and Tianwen-3 mission (Beaty et al., 2019; Haltigin et al., 2022; Shen et al., 2022). At Gale Crater, Curiosity rover encountered multiple diagenetic structures such as calcium sulfate veins, nodules, and concretionary textures in fluvial-lacustrine deposits (Stack et al., 2014). Previous studies suggested that the nodules at Gale Crater could contain evaporitic, Fe-bearing, and clay minerals, and could precipitate in saline and alkaline-neutral pore waters (Grotzinger et al., 2014; McLennan et al., 2014; Vaniman et al., 2014). They could form in evaporitic lacustrine environments related to the process of surface aridification (Stack et al., 2014; Wiens et al., 2017; Sun et al., 2018; Rapin et al., 2019). The nodules have been proposed as a favorable taphonomic window for biosignature preservation due to the early lithification of concretionary structure (Stack et al., 2014; Grice et al., 2019). Previous studies have reported organic matter, fossils, biominerals, and isotopic biosignatures preserved within nodules formed in marine settings or terrestrial freshwater systems (e.g., Marshall and Pirrie, 2013; Plet et al., 2020; Loyd et al., 2023). As for playa nodules, biomass could be low in saline diagenetic fluids considering low productivity and buried biomass in evaporitic lacustrine environments (Kong et al., 2014; Shkolyar and Farmer, 2018; Chen et al., 2022; Azua-Bustos et al., 2023). Low biomass could be significantly influenced by the diagenetic environments and burial conditions (Summons et al., 2011). Nevertheless, the influences on the preservation of biosignatures within playa nodules have not been investigated, including possible preservation of biogenic textures, biominerals, carbonaceous materials, and chemical features indicative of biological processes.

Massive carbonate nodules precipitating from early-diagenetic briny waters were discovered in the hyperarid western Qaidam Basin (Sun et al., 2021). The western Qaidam Basin is an important Mars analog field site with an average annual precipitation of less than 20 mm and an aridity index of 0.01–0.05 currently (Yang, 1986; Zheng et al., 2002; Kong et al., 2018). It had lakes and rivers on the surface from the Oligocene to Pleistocene, but then lost its water due to the uplift of the Tibetan Plateau and progressive surface aridification (Yin et al., 2008a; Yin et al., 2008b; Li J. et al., 2016). The western Qaidam Basin has thus developed various Mars-like geomorphologies, including dunes, yardangs, gullies, alluvial fans, playa deposits, and polygons (Anglés and Li, 2017; Xiao et al., 2017; Antunes et al., 2023). These aridification processes in the western Qaidam Basin can also be analogous to those on Mars during the Noachian-Hesperian transition (Shen et al., 2022). The carbonate nodules outcropped in the foreland basin of Altun Mountain within the mid-Pleistocene saline lacustrine sediments (Sun et al., 2021; Chen et al., 2023). They were mainly composed of carbonate minerals with minor contributions from quartz, feldspar, and evaporite minerals and were considered to form in salty pore waters related to ephemeral playa lakes in the arid climate (Han et al., 2014; Sun et al., 2021). While the mineral compositions of the Qaidam nodules differ from those found at Gale Crater, they could still be analogous to nodules at Gale Crater on Mars based on their formation backgrounds.

In this study, we utilize a comprehensive suite of techniques, including microscopy, spectroscopy, mass spectrometry, and elemental analyses, to characterize the Qaidam nodules. Through an examination of their textural, isotopic, mineralogical, and organic matter features, alongside the published total organic carbon (TOC) contents in the surrounding fluvio-lacustrine deposits within the Qaidam Basin, we elucidate the taphonomy of biosignatures in these nodules. The results of this study provide guidance for the detection of potential biosignatures in nodules at Gale Crater on Mars.

2 Materials and methods

2.1 Sampling

The carbonate nodule field was located in the western Qaidam Basin (38.45°N–38.48°N, 92.14°E–92.15°E), China, one of the largest and driest deserts in the world (Figure 1A,B). The nodules outcropped within the mid-Pleistocene lacustrine strata (Sun et al., 2021; Chen et al., 2023), bordering flat playa deposits to the north and salt crust to the south (Figure 1C). They mostly occurred as aggregates in the shape of domes cemented by gypsum and halite (Figure 1C,D). The primitive lacustrine sediments surrounding nodules were not often observed, and most of them were altered and cemented by evaporite minerals. This region was wind-eroded, leaving nodule domes, yardangs, aeolian dust, and sands on the surface. The carbonate nodules had spherical, ellipsoidal, subangular, and planar shapes with sizes ranging from millimeters to centimeters (Figure 1D; Figure 2). They often consisted of inner cores and outer bands with alternating colors and textures. Some nodules did not contain cores or had multiple growing centers.

In this study, surface regolith and nodules of different shapes and sizes were collected (Figure 2). Weathered fragments and

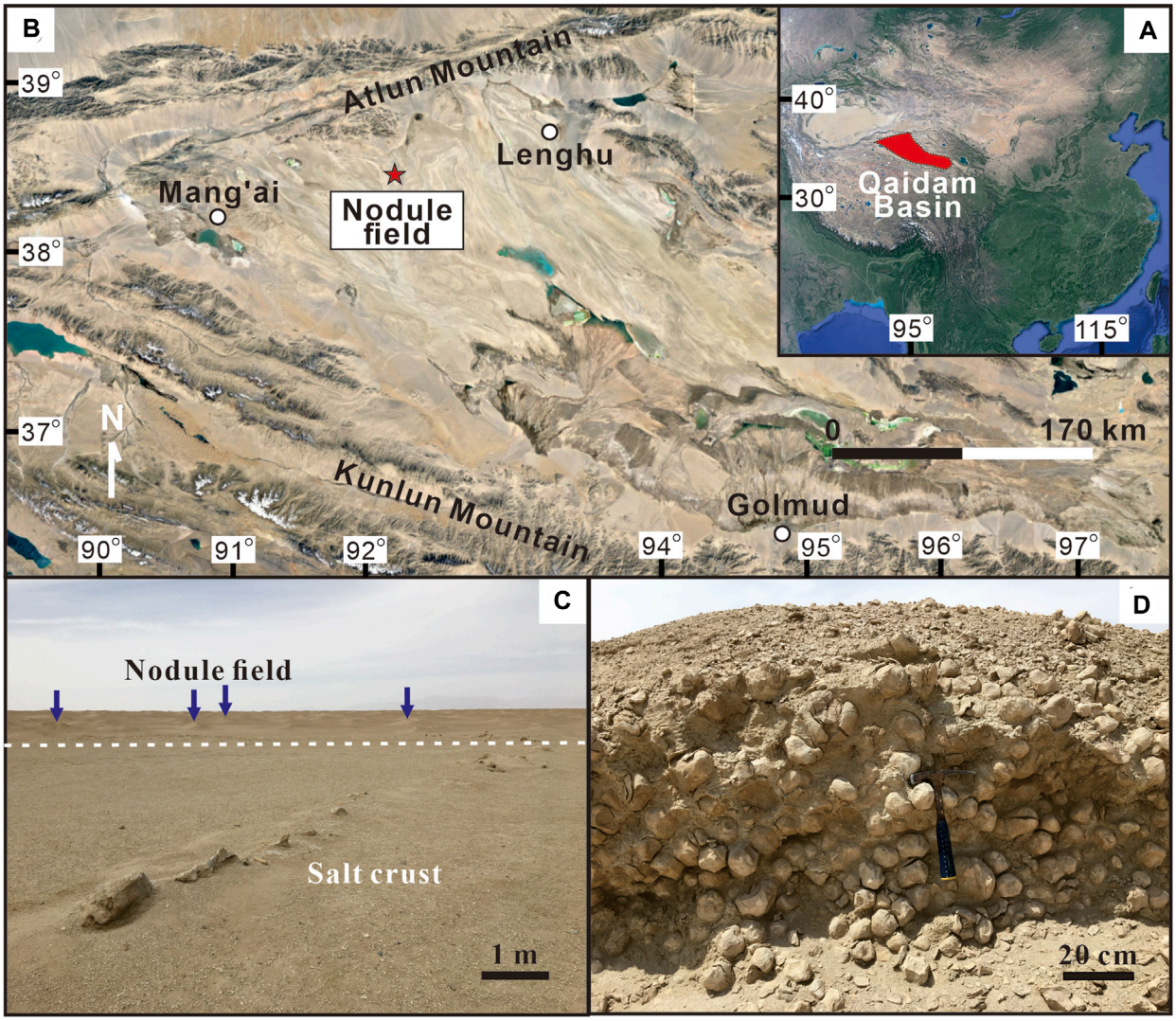

FIGURE 1
Location and landscapes of the nodule field. **(A)** Location of the Qaidam Basin in China (red area). **(B)** Location of the nodule field (red star) in the enlargement of the Qaidam Basin. **(C)** The south end of the nodule field indicated by a white dash line. To the south of the nodule field was the salt crust. The nodules outcropped in the shape of a dome (blue arrows) in the distance. **(D)** Cross-section of a dome showing nodule aggregates inside.

large veins in nodules were avoided during field sampling and laboratory analyses because they were thought to influence primitive biosignature preservation. Rock slabs and polished thin sections were prepared for both microscopic and spectroscopic analyses, while pulverized samples were prepared for elemental and isotopic analyses. Specifically, the nodule was cut in half. A second cut was parallel to the first one to get ~5 mm thick slabs using a diamond wire saw cutting machine (Shenyang Kejing Auto Instrument Corporation, Shenyang, China). The surface of the rock slab was then polished on a silicon carbide polishing disc and milled by a broad Ar-ion beam in Leica EM TIC 3X (Leica Microsystems GmbH, Wetzlar, Germany) to remove contamination on the surface before analyses. Polished thin sections were made with a thickness of approximately 30 μm to show the internal structures and textures of nodules. Pulverized samples were drilled from polished slabs using a Strong 90 Lab Dental Micro motor handpiece drill with a 1.5-mm-diameter bit (STRONG, Fujian, China). The obtained samples were then pulverized in a clean agate mortar.

2.2 Optical microscopy

Microfabrics analyses in carbonate nodules were performed with light microscopy on polished thin sections and rock slabs. Transmitted light optical microscopy was performed on polished thin sections using a Nikon Eclipse LV100N POL polarizing microscope (Nikon Corporation, Tokyo, Japan). Reflected light images were taken on the polished surface of each rock slab with a Zeiss Smartzoom five automated digital microscope (Carl Zeiss Microscopy GmbH, Jena, Germany) for region selection in later analyses.

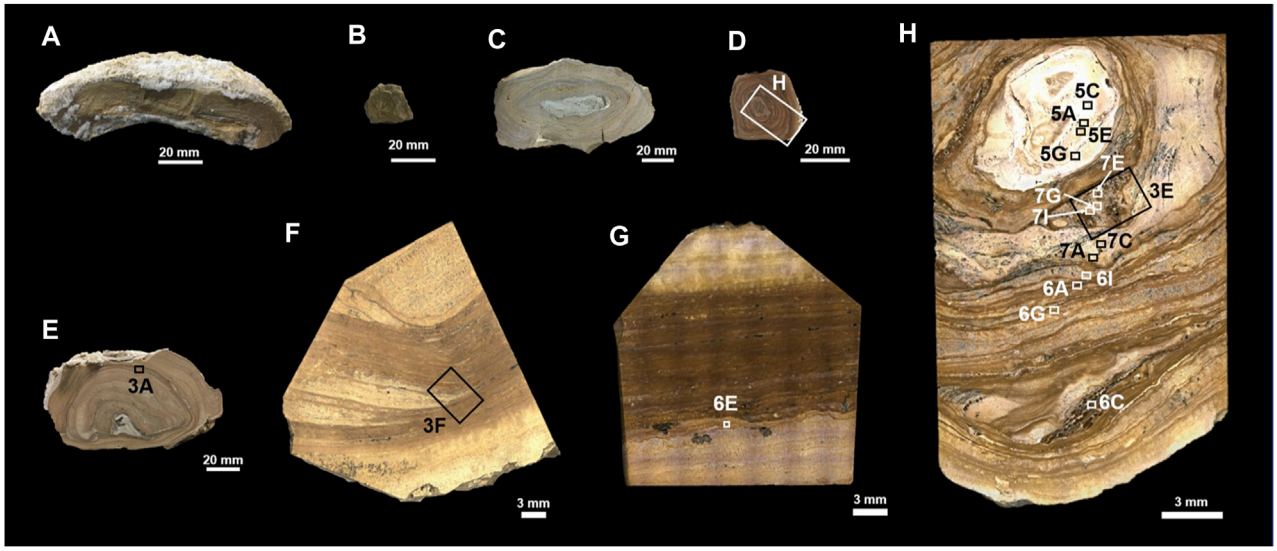

FIGURE 2
Overview of carbonate nodules of different shapes and sizes from the western Qaidam Basin. **(A)** A nodule specimen with an almost planar shape. **(B)** A nodule with a subangular shape. **(C–E)** Nodules with spherical and ellipsoidal shapes. The nodule in panel **(C)** has been mentioned in Chen (2023). **(F–H)** Different sections from the nodules. The rock slab in panel **(H)** represents the region of the white frame in panel **(D)**. The black frames in panels **(E, F, H)** represent the regions in Figures 3A, E, F, respectively. The small frames in panels **(G, H)** represent the regions in Figures 5–7.

2.3 Scanning electron microscopy (SEM)

SEM was performed using backscattered electron (BSE) mode on the polished surface of the rock slab with a Thermo Scientific Apreo S LoVac scanning electron microscope (Thermo Fisher Scientific Incorporation, Waltham, United States). Working conditions for SEM imaging involved an accelerating voltage of 1–2 kV, an electron beam current of 0.1–0.2 nA, and a working distance of 8–10 mm using the T1 detector.

2.4 Raman spectroscopic analysis

Raman imaging and spectroscopy were acquired on the polished rock slabs using a WITec Alpha 300R confocal Raman imaging system (Witec GmbH, Ulm, Germany). A laser of 532 nm wavelength was used in this study, with a diffraction grating of 300 grooves/mm, and a spectral resolution better than 6 cm^{-1}. Samples were targeted using a high magnification (×50 or ×100) objective with a spot size of ≤1 μm (Li et al., 2023). Raman spectra were obtained typically with 30 accumulations, 1 s dwell time, a maximum 3 mW laser power, and a 0–4,000 cm^{-1} shift range. As for suspected carbonaceous materials, a laser beam with a power of 1 mW to avoid surface burning was focused underneath the polished surface to avoid contamination and polishing artifacts (Beyssac et al., 2003). A linear baseline in the region of 1,000–1800 cm^{-1}, which contains first-order bands characteristic of bond vibrations from carbonaceous materials, was used to remove the background fluorescence to acquire intensities of organic bands (Kouketsu et al., 2014; Bonoldi et al., 2016). The spectra were analyzed in OriginPro 2024 (Learning Edition, OriginLab Corporation, Northampton, MA, United States).

2.5 TOC contents and organic carbon isotope ($\delta^{13}C_{org}$) analyses

Analyses of TOC and $\delta^{13}C_{org}$ were performed on decarbonated sample powders drilled from cores and bands in different nodules. Before analyses of TOC content and $\delta^{13}C_{org}$, 1–2 g of unaltered sample powders were dissolved in 3 M HCl for 12 h to remove carbonate minerals, rinsed to pH-neutral, and dried (Chen et al., 2022). The weights of decarbonated solid residues were recorded for subsequent TOC content calculation. Organic carbon contents were measured by an NC Technologies ECS4024 elemental analyzer (NC Technologies, Milano, Italy). Results were calibrated against the reference material IVA33802150, with a precision of 0.7%. Determination of $\delta^{13}C_{org}$ was performed using a Thermo 253 Plus Isotope Ratio Mass Spectrometer (IRMS) coupled to an elemental analyzer (Thermo Fisher Scientific, Bremen, Germany). The values were expressed in per mil notation relative to Vienna PeeDee Belemnite (VPDB). The analytical precision of the $\delta^{13}C_{org}$ measurement was within ±0.2‰ based on multiple measurements of reference material (Elemental Microanalysis B2153).

2.6 Inorganic carbon isotope ($\delta^{13}C_{carb}$) and oxygen isotope ($\delta^{18}O_{carb}$) analyses

Untreated crushed samples were acidified with anhydrous phosphoric acid under vacuum for 24 h at 25°C. The evolved CO_2 was purified and fed into a ThermoFisher Scientific MAT-253 IRMS (Thermo Fisher Scientific, Bremen, Germany). Isotopic compositions were reported in per mil notation relative to the VPDB standard. The reproducibility for $\delta^{13}C_{carb}$ and $\delta^{18}O_{carb}$ were better than ±0.15‰ and ±0.20‰, respectively, based on multiple measurements of a laboratory internal standard.

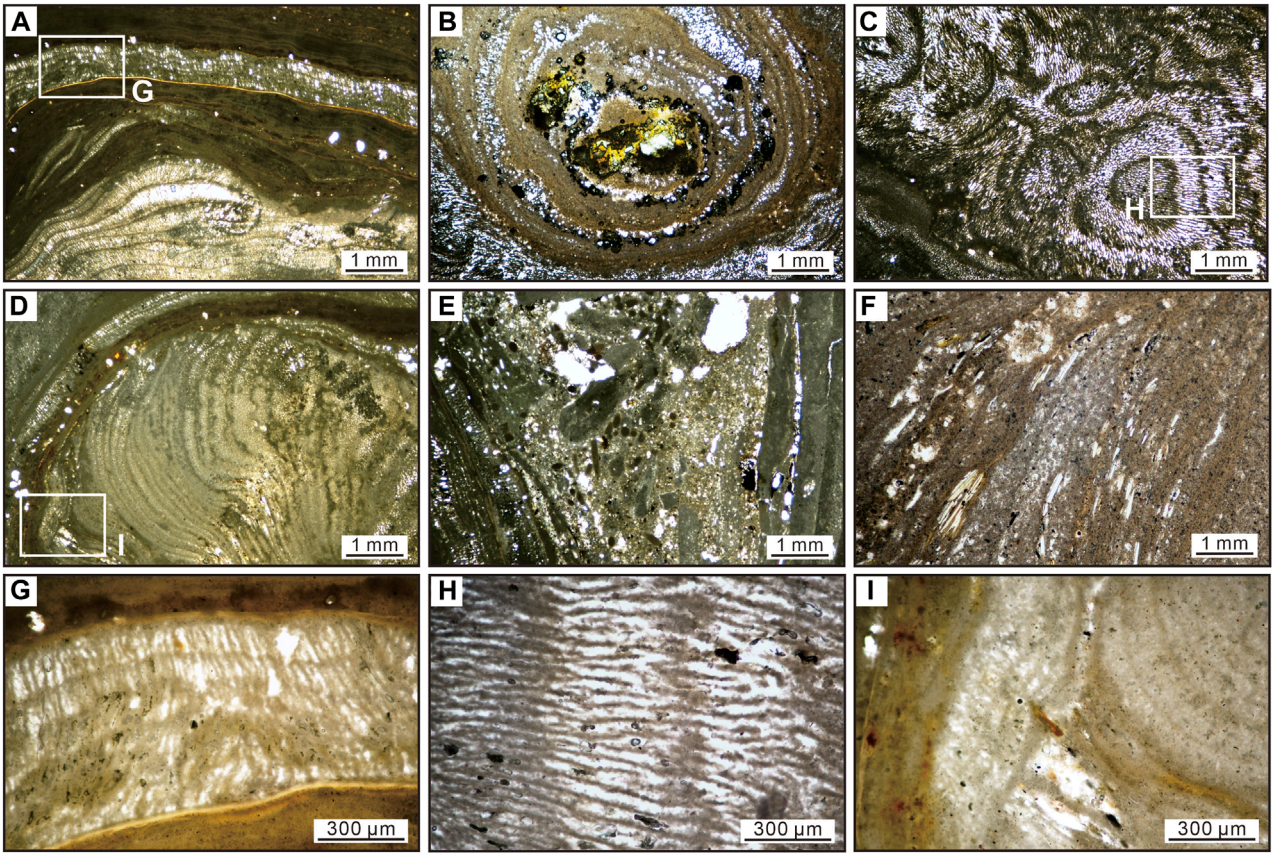

FIGURE 3
Photomicrographs images of microfabrics within carbonate nodules in this study under plane-polarized transmitted light (TL). **(A)** A TL image of the boxed zone in Figure 2E shows micrite-dominated and sparite-dominated bands, corresponding to the light and dark bands respectively. **(B)** A cross-section of the nodule **(B)** in Figure 2 shows a concentric zoned structure. **(C)** A cross-section of the nodule with multiple cores shows an irregular growing pattern of zoned structures inside. **(D)** A TL image showing micrite texture in the porous light bands of zoned structures. **(E)** A TL image of the boxed zone in Figure 2H shows the occurrence of detrital minerals in nodules. **(F)** A TL image of the boxed zone in Figure 2F shows the occurrence of detrital minerals in the micrite matrix. **(G)** An enlargement of a sparite-dominated band in panel **(A)** showing radial-fibrous texture. **(H)** Close-up of the white box in panel **(C)** showing alternate micrite and sparite that is composed of radial-fibrous texture. **(I)** Close-up of the white box in panel **(D)** showing micrite texture in porous light bands.

3 Results

3.1 Microscopic observations of the Qaidam nodules

The zoned structures of nodule samples consist of porous light bands and compact dark bands as identified in previous studies (Figure 2C–H; Sun et al., 2021; Chen et al., 2023). Plane-polarized transmitted light images of zoned structures show that compact dark bands are composed of micrite while porous light bands are primarily sparite (Figures 2, 3A,B,G). A cross-section of a nodule with multiple cores shows that zoned structures grow in different directions in one nodule, but still exhibit alternating micrite-dominated and sparite-dominated bands in different zoned structures (Figure 3C,H). Nevertheless, porous light bands can also consist of micrite (Figure 3D,I). The sparite is mainly comprised of radial-fibrous carbonate minerals (Figure 3A–C,G,H). Close-up images of the nodules show that some bands also contain detrital minerals (Figure 2H; Figure 3E,F). The bands can also grow asymmetrically, with uneven growth thickness and curvature (Figure 3A,D).

In the SEM-BSE images, dispersed dark materials which might be organic matter can be found in cores and zoned structures (Figure 4). They mainly present as small particles—with maximum diameters from <1 μm to dozens of micrometers. These particles are often observed as massive (length/width ratio <15; Figure 4E, F), filamentous (length/width ratio >15; Figure 4C,D), and annular structures (Figure 4A,B).

3.2 Spectroscopic and geochemical characteristics of the Qaidam nodules

As the Qaidam nodules contain cores, alternating light porous and dark compact bands, and bands containing big detrital minerals that could form in different environments (Figure 2; Figure 3), we performed spectroscopic and geochemical analyses on the above-mentioned different components of the Qaidam nodules.

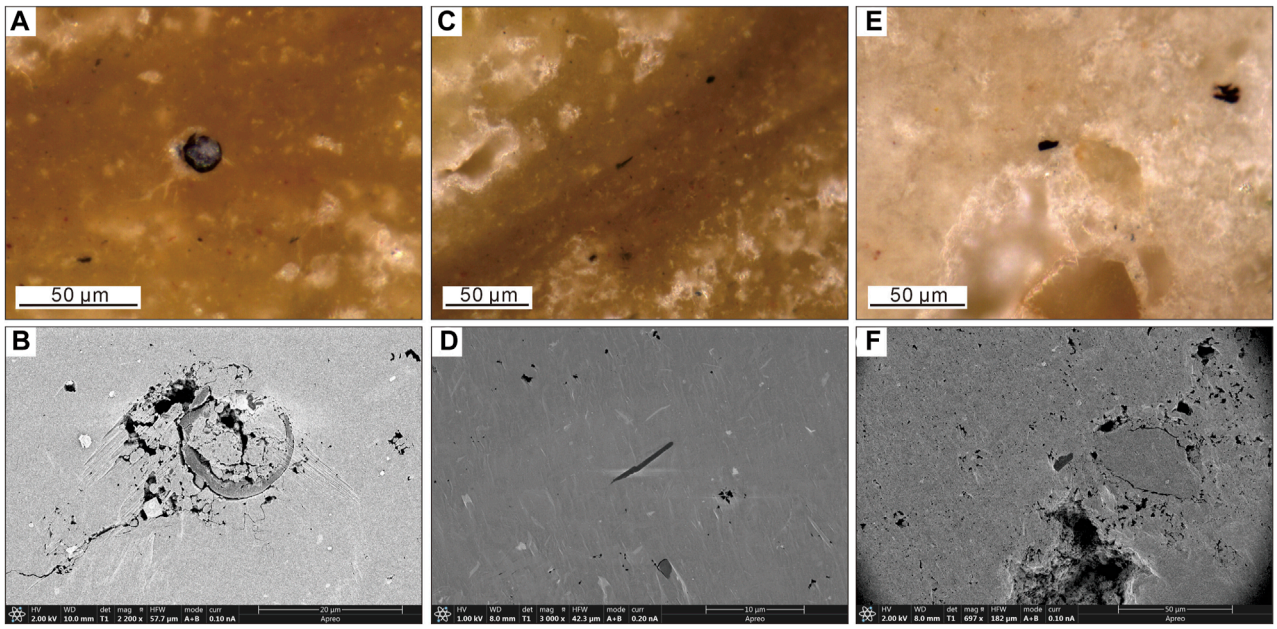

FIGURE 4
ZEISS Smartzoom reflected light photomicrographs **(A,C and E)** and SEM-BSE images **(B,D and F)** of the dispersed dark materials in the Qaidam nodules. **(A and B)** Show a transection of an annulus with a diameter of <20 μm. The inner bore and outer side of the annulus are filled with minerals. **(C and D)** Needle-like dark materials with a length of ~10 μm and a width of ~0.5 μm. **(E and F)** Massive dark materials with a size of ~10 μm.

3.2.1 The cores of the Qaidam nodules

The carbonate matrix in the cores of the nodules is mainly composed of aragonite with minor contributions from dolomite and magnesian calcite as suggested by Raman spectra (Figure 5 and Supplementary Appendix S1). This is consistent with previous results analyzed by X-ray diffraction (XRD) (Sun et al., 2021), which also suggested aragonite as the main component. Apart from the carbonate matrix, there are also detrital minerals such as quartz, orthoclase, muscovite, anatase, and actinolite in the cores of the nodules. As for dark particles observed in SEM-BSE images, Raman spectra suggest that most of them are opaque minerals. An observation of a small number of dark particles with bands at ~1,350 and ~1,600 cm^{-1} suggests that some of them are disordered carbonaceous materials (Figure 5; Foucher, 2019). The intensity ratio of 1,350 vs 1,600 cm^{-1} bands in Raman spectra, defined as I-1350/1,600, has a range of 0.65–0.78 and an average of 0.74 after background subtraction (Table 1 and Supplementary Appendix S1). The TOC contents and $\delta^{13}C_{org}$ in cores have ranges of 0.01%–0.09% (averaged 0.05%) and −23.9‰ to −24.7‰ (−24.3‰), respectively (Table 2).

3.2.2 The light porous and dark compact bands of the Qaidam nodules

The carbonate matrix in the light porous and dark compact bands of the nodules is mainly composed of magnesium calcite (Figure 6 and Supplementary Appendix S1), consistent with previous XRD results (Sun et al., 2021). There are different degrees of addition of magnesian to calcite matrix, as revealed by shifts at bands of ~170, ~290, and ~1,090 cm^{-1} in Raman spectra. The calcite matrix sometimes contains quartz, phlogopite, and hematite. The $\delta^{13}C_{carb}$ and $\delta^{18}O_{carb}$ in light bands are 2.1‰ and −0.9‰ to −1.7‰, respectively, while they are 2.1‰ and −0.4‰, respectively, in dark compact bands. As revealed by bands at ~1,350 and ~1,600 cm^{-1} in Raman spectra, the dark particles are organic matter (Figure 6). They present as black massive and annular structures and are mostly embedded in a magnesium calcite matrix. The I-1350/1,600 data of organic matter in light and dark bands have a range of 0.73–1.02 and an average of 0.86 after background subtraction (Table 1 and Supplementary Appendix S1). The average I-1350/1,600 in dark bands (0.88) is higher than that in light porous bands (0.78). The TOC contents and $\delta^{13}C_{org}$ in dark bands range from 0.04% to 0.15% (averaged 0.09%) and from −23.5‰ to −27.4‰ (averaged −24.9‰), respectively (Table 2). The TOC contents and $\delta^{13}C_{org}$ in light bands range from 0.04% to 0.56% (averaged 0.16%) and from −22.7‰ to −29.3‰ (averaged −25.4‰), respectively.

3.2.3 The bands containing big detrital minerals in the Qaidam nodules

The carbonate matrix in the zoned structures containing big detrital minerals is mainly composed of magnesium calcite (Figure 7 and Supplementary Appendix S1). It sometimes contains detrital minerals such as actinolite, anatase, quartz, clinochlore, albite, and hornblende according to Raman spectra, consistent with previous XRD results (Sun et al., 2021). Raman spectra show the occurrence of carbonaceous materials with bands at ~1,350 and ~1,600 cm^{-1} and bands attributed to C–H stretching vibrations at 2,800–3,000 cm^{-1} (Figure 7; Snyder et al., 1978; Foucher, 2019). These carbonaceous materials are often observed to be associated with detrital carbonate and silicate minerals. The I-1350/1,600 data of organic matter range from 0.19 to 1.28 with an average of 0.69 after background subtraction (Table 1 and Supplementary Appendix S1).

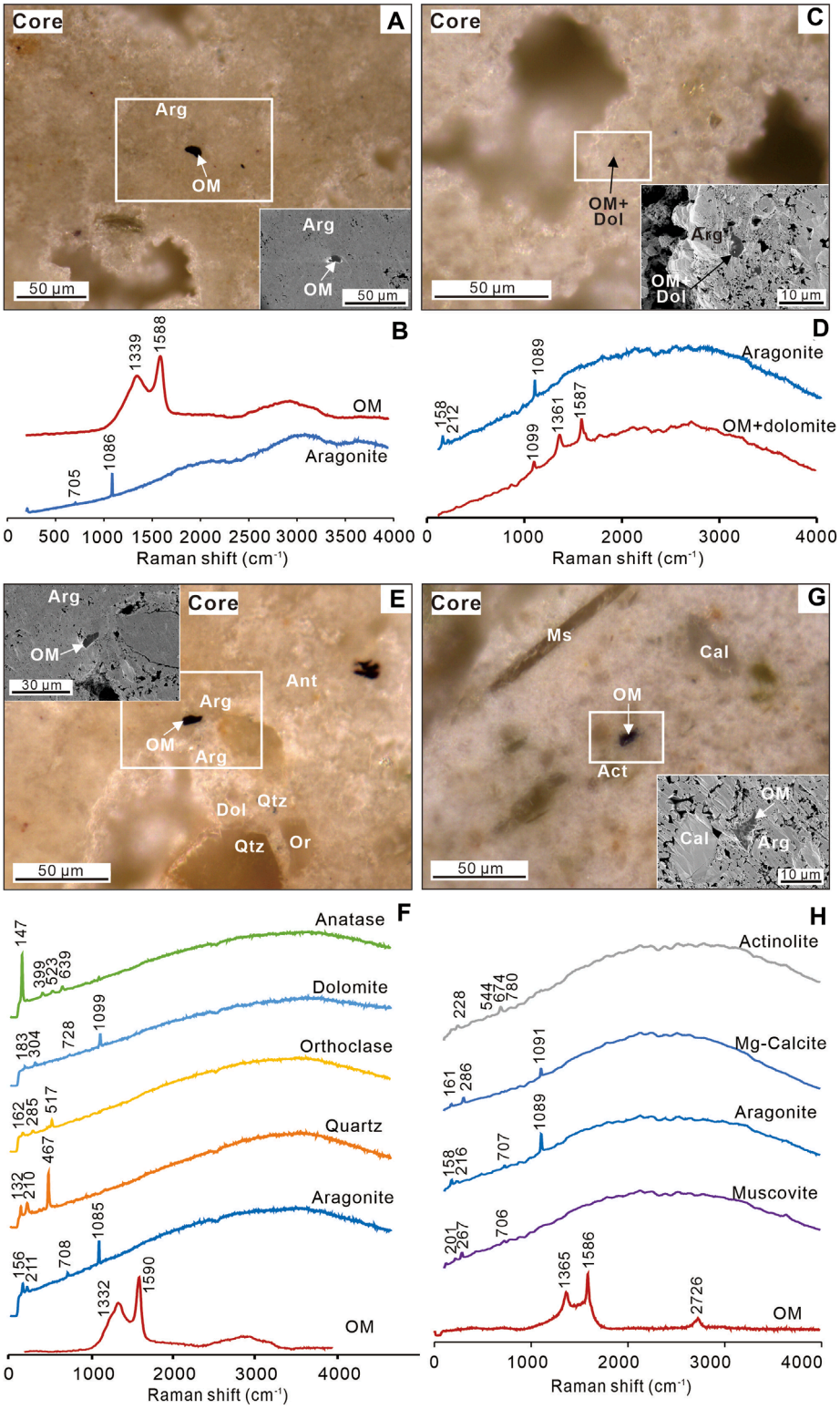

FIGURE 5
Organic matter mineral assemblages in cores of carbonate nodules. **(A,C,E and G)** ZEISS Smartzoom reflected light (RL) images of organic matter. Insets are SEM-BSE images of the white-boxed areas in RL. **(B,D,F and H)** Representative Raman spectra for respective photomicrographs. Qtz = quartz; OM = organic matter; Cal = Mg-calcite; Arg = aragonite; Dol = dolomite; Ant = anatase; Or = orthoclase; Act = actinolite; Ms = muscovite.

TABLE 1 The intensity ratios of 1,350 vs 1,600 cm^{-1} bands (I-1350/1,600) for analyzed carbonaceous materials. The "H" and "G" denote nodules in panels "H" and "G" in Figure 2. The "dark", "light", and "detritus" denote "dark bands", "light bands", and "bands containing big detrital minerals," respectively.

Location of the nodule	Microphotograph	I-1350/1,600
H-Core	Figure 5A	0.76
H-Core	Figure 5C	0.76
H-Core	Figure 5E	0.78
H-Core	Figure 5G	0.65
H-Dark	Figure 6A	0.73
H-Dark	Figure 6C	1.02
G-Dark	Figure 6E	0.94
H-Dark	Figure 6G	0.82
H-Light	Figure 6I	0.78
H-Detritus	Figure 7A	0.19
H-Detritus	Figure 7C	0.76
H-Detritus	Figure 7E	1.28
H-Detritus	Figure 7G	0.54

4 Discussion

We characterize the biosignatures in the Qaidam nodules from the perspectives of macro- and micro-textural, geochemical, mineralogical, and organic records (Hays et al., 2017). Organic matter is found in the Qaidam nodules by SEM and Raman spectroscopic analyses (Figure 5–7), consistent with the results from a previous study (Chen et al., 2023). The TOC content of the Qaidam nodules has an average value of 0.10% (Table 2), slightly higher than that of fluvio-lacustrine deposits (0.07%) in the hyperarid Qaidam Basin (Chen et al., 2022). Most of the organic matter has been considered to be sourced from *in-situ* biomass in diagenetic fluids (Chen et al., 2023). Higher TOC content in the Qaidam nodules as compared to that in fluvio-lacustrine deposits suggests that terrestrial playa nodules could offer conducive conditions for biomass preservation in spite of possibly low productivity levels in diagenetic environments (Meyers and Ishiwatari, 1993). Besides, an organic annulus with a diameter of less than 20 μm in a dark compact band has been observed (Figure 6E). The annulus is likely a cross-section of an organic spherule, which may represent a fossil spore based on its general characteristics in morphology and size (Balme, 1995; Saxena et al., 2021), or represents a microtubule—an algal filament microfossil (Butterfield et al., 1990; Knoll et al., 2007). The inner bore and outer edge of the annulus are filled with magnesium calcite with a minor contribution from organic matter, suggesting possible rapid entombment by mineral cementation during cellular lysis and degradative processes (Figure 6F; McMahon et al., 2018). The TOC level of zoned structures with a range of 0.04–0.56% and an average of 0.12%, is generally higher than that of the cores (0.01–0.09% and 0.05%) in nodules (Table 2). Lower TOC level in cores could result from low biomass in waters where cores precipitated. A previous study has implicated more saline diagenetic environments (Sun et al., 2021), which could be unfavorable for microbial growth (Yan et al., 2015; Velthuis et al., 2023). Alternatively, organic matter in cores could have experienced more post-depositional alteration as suggested by the formation process of the Qaidam nodules (Sun et al., 2021).

The macro- and micro-textures the carbonate minerals suggest that the Qaidam nodules could be of biogenic origin. The zoned structures of the Qaidam nodules could be formed by the accretion of adhesive debris caused by the secretion of mucus by algae-dominated microorganisms (Figure 2; Figure 3). Previous studies have found the important roles of extracellular polymeric substances (EPS) in precipitating micritic layers and alternating sparry and micritic layers in common carbonate cements (e.g., Pedley, 1992; Arp et al., 2001; Dupraz et al., 2004). Carbonate crystal nucleation may take place on EPS to form micrite-sized dendrites, which could then be completely replaced by solid and syntaxial carbonate crystals (Pratt, 1976; Turner and Jones, 2005). The alternating occurrence of micritic and sparry to fibrous crystals of carbonate minerals may depend on the spacing of individual dendrite crystal domains and the ensuing growth thickness of dendrites. Also, the fibrous nature and *c*-axis orientation of crystal growth could be related to the EPS characteristics (Turner and Jones, 2005; Yang et al., 2022). Hence, the growth of micrite and sparite layers with radial-fibrous textures in zoned structures might be related to carbonate precipitation captured or trapped by algae (Figure 2; Figure 3A–C,G,H).

TABLE 2 TOC, $\delta^{13}C_{org}$, $\delta^{13}C_{carb}$, and $\delta^{18}O_{carb}$ for different cores and bands in carbonate nodules. Samples surface regolith, S1, and S2 refer to the surface regolith, Nodule S1, and S2, respectively, which have been mentioned in Chen (2023). Samples E and F refer to Nodules (E) and (F) respectively in Figure 2. Suffixes "dark" and "light" denote "dark bands" and "light bands," respectively.

Sample no.	TOC (%)	$\delta^{13}C_{org}$ (‰ PDB)	$\delta^{13}C_{carb}$ (‰ PDB)	$\delta^{18}O_{carb}$ (‰ PDB)
S1-light	0.11	−25.1	2.4	−0.9
S1-dark	0.14	−26.0	2.1	−0.4
S1-core	0.01	−23.9	—	—
S2-light	0.14	−26.0	2.4	−1.7
S2-dark	0.15	−24.8	—	—
S2-core	0.09	−24.2	—	—
Surface regolith	0.04	−27.5	—	—
E-light	0.06	−22.7	—	—
E-dark	0.06	−24.1	—	—
E-core	0.05	−24.7	—	—
F-light	0.56	−29.3	—	—
F-dark	0.09	−27.4	—	—
N1-light	0.04	−24.7	—	—
N1-dark	0.05	−23.5	—	—
N2-light	0.04	−24.5	—	—
N2-dark	0.04	−23.7	—	—

Nevertheless, these fabrics in the Qaidam nodules can also originate from abiotic processes (Grotzinger and Rothman, 1996; Kano et al., 2019). The lamination and radial-fibrous textures of the spring carbonate deposits could reflect temporal changes in local physical and chemical factors (Grotzinger and Rothman, 1996; Bosak et al., 2021). In addition, the carbonate minerals of these Qaidam nodules as indicated in a previous study are present as rhombic aggregates and do not exhibit microfabrics attributed to microfossils, biofilms, or microbial activities in zoned structures of nodules (Sun et al., 2021). They are also not depleted in ^{13}C as compared to those in contemporary saline lacustrine deposits (Table 2; Han et al., 2014; Li X. et al., 2016; Chen et al., 2020). This further suggests the importance of physicochemical processes in the precipitation of carbonate minerals (Wagner et al., 2018). In sum, there is no strong evidence supporting the biogenicity of the Qaidam nodules, although the possibility of biologically mediated or induced precipitation of nodules cannot be fully excluded based on previous works in Franconian Alb, Germany (e.g., Pratt, 1976; Arp et al., 2001), which suggested the cooccurrence of cyanobacteria-diatom biofilms and sparry and micritic calcite in cold-water tufa formed at cool springs and in creeks.

The I-1350/1,600 values of carbonaceous materials in the Qaidam nodules carry information derived from their organic precursors and the subsequent post-depositional alterations they have experienced (Figure 8; Table 1). The I-1350/1,600, which is applied to characterize the structural order of carbonaceous materials (Buseck and Beyssac, 2014; Foucher et al., 2015), has a range of 0.19–1.28 for the Qaidam nodules (Figure 8; Table 1). The structural order is influenced by the molecular structures of organic precursors, post-depositional processes such as thermal alteration, hydrothermal fluid alteration, deformation and shear force, and mineral-templating effects inducing graphitization on the surfaces of quartz/chlorite minerals (e.g., Franklin and Randall, 1951; van Zuilen et al., 2012; Kouketsu et al., 2014). Previous studies have indicated that carbonaceous materials subjected to metamorphic changes exhibit unique Raman spectra (Beyssac et al., 2002; Kouketsu et al., 2014). Most of the I-1350/1,600 data in cores, dark and light bands exhibit moderate values (0.65–1.02; Figure 5–8). This suggests that thermal alterations may be not significant. Also, there is no obvious veining in the Qaidam nodules indicating post-depositional fluid alteration (Figure 2). Most of the organic matter is homogeneously embedded in carbonate minerals, and thus I-1350/1,600 variation cannot be explained by mineral templating effects (Figure 5–8; van Zuilen et al., 2012). The lack of a significant difference in I-1350/1,600 data among different components of the Qaidam nodules (p = 0.81), as revealed by the analysis of variance (ANOVA), further eliminates the possibility

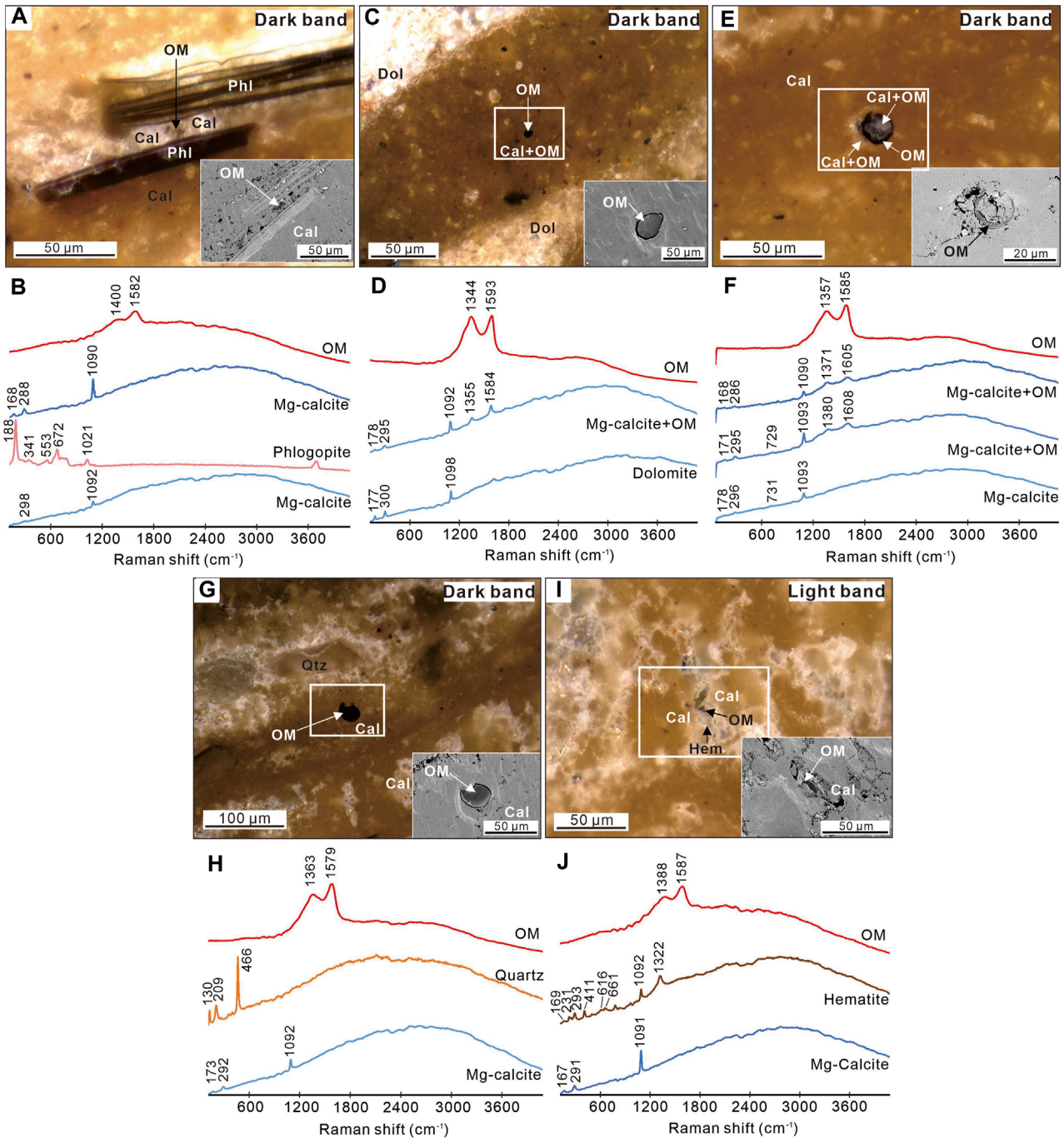

FIGURE 6
Organic matter mineral assemblages in light porous and dark compact bands of carbonate nodules. **(A,C,E,G and I)** ZEISS Smartzoom reflected light (RL) images of organic matter. Insets are SEM-BSE images of the white-boxed areas or the same area in RL. **(B,D,F,H and J)** Representative Raman spectra for respective RL images. Qtz = quartz; OM = organic matter; Cal = Mg-calcite; Dol = dolomite; Phl = phlogopite; Hem = hematite.

of local post-depositional alterations on carbonaceous materials (Figure 8). Nevertheless, carbonaceous materials exhibiting highly variable I-1350/1,600 values (0.19–1.28) within detritus-containing bands may involve detrital organic matter characterized by higher levels of metamorphism. Therefore, apart from minor detrital sources, the I-1350/1,600 values indicate that carbonaceous materials in the Qaidam nodules could primarily originate from carbon precursors of various subcellular components or coexisting organisms present in diagenetic waters (Figure 8; Table 1; Franklin and Randall, 1951; Sforna et al., 2014; Foucher et al., 2015). This inference is consistent with previous Fourier transform infrared (FTIR) spectroscopy analyses on the Qaidam nodules which suggested the involvement of diverse microbial communities in diagenetic waters (Chen et al., 2023).

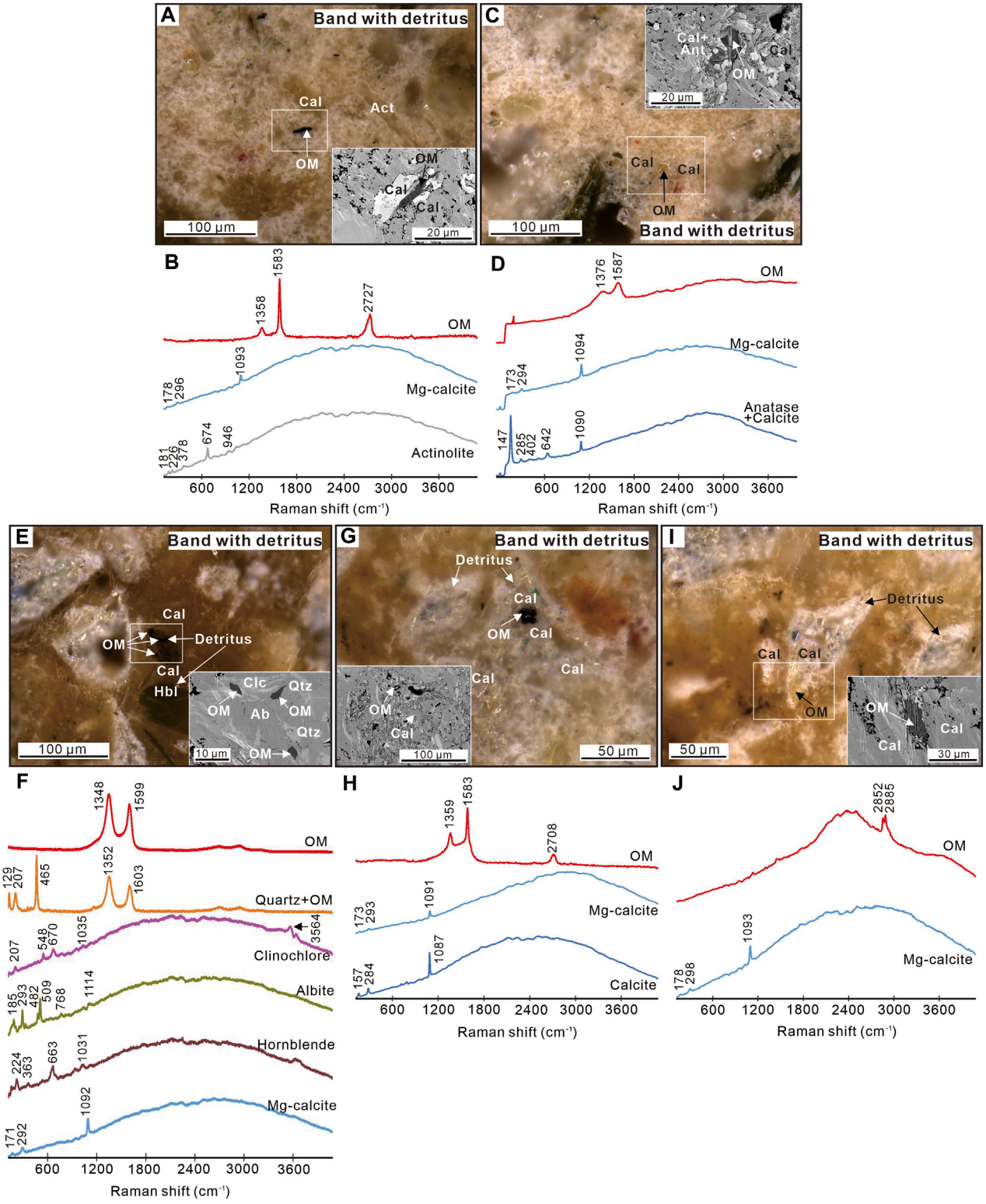

FIGURE 7
Organic matter in bands with big detrital minerals. **(A,C,E,G and I)** ZEISS Smartzoom reflected light (RL) images of organic matter. Insets are SEM-BSE images of the white-boxed areas or the same area in RL. **(B,D,F,H and J)** Representative Raman spectra for respective RL images. OM = organic matter; Cal = Mg-calcite; Ant = anatase; Act = actinolite; Qtz = quartz; Ab = albite; Hbl = hornblende; Clc = clinochlore.

The $\delta^{13}C_{org}$ records in the Qaidam nodules provide further evidence for carbon fixation pathways metabolized by dominant primary producers. Carbon fixation produces distinct isotopic fractionation due to isotopic discrimination between ^{12}C and ^{13}C by the carboxylating enzymes in biomass (Hurley et al., 2021). Different carbon fixation pathways have different characteristic fractionations.

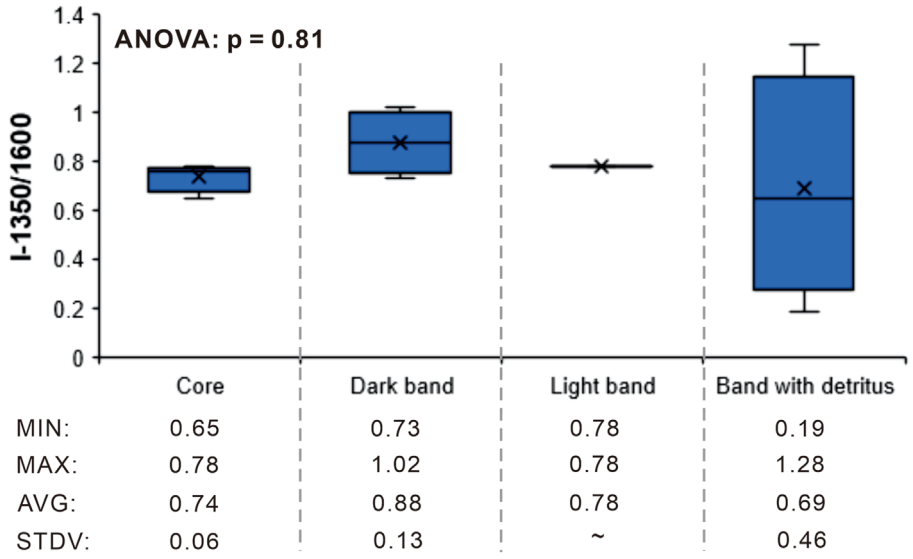

FIGURE 8
Distribution of the intensity ratios of 1,350 vs 1,600 cm^{-1} bands (I-1350/1,600) in different components of the Qaidam nodules, summarized from Figure 5–7 and Table 1. The averaged, maximum, and minimum values as well as standard deviation of I-1350/1,600 data for each group are illustrated below the graph.

The Wood-Ljungdahl pathway imparts the largest fractionation (>30‰), the Calvin cycle results in less fractionation (20–30‰), and rTCA and other pathways produce the least fractionation (0–12‰) (Hügler and Sievert, 2011; Freude and Blaser, 2016; Ward and Shih, 2019). The $\delta^{13}C_{org}$ values ranging from −22.7‰ to −29.3‰ and $\delta^{13}C_{carb}$ values ranging from 2.1‰ to 2.4‰ in zoned structures are consistent with carbon fixation pathways of the Calvin cycle using Rubisco or the Wood-Ljungdahl pathway (Table 2).

Multiple diagenetic structures such as nodules and concretionary textures have been identified in fluvial-lacustrine deposits at Gale Crater on Mars (Gasda et al., 2022). Although nodules at Gale Crater do differ from those in the Qaidam Basin regarding their mineral compositions, they are comparable regarding their forming backgrounds and post-depositional processes. Therefore, it is reasonable to speculate biosignatures including carbonaceous materials and even microfossils to be preserved in nodules at Gale Crater if life ever evolved on Mars. Nevertheless, it should be noted that Mars's surface environments could be more hostile and extreme, and the search for biosignatures on Mars could be more difficult. The Mars Sample Return campaign is necessary by bringing back Martian rocks and soils to Earth for detailed investigation using all the capabilities of terrestrial laboratories.

5 Conclusion

Saline diagenetic fluids in terrestrial playa environments may contain low levels of biomass, and the preservation of biomass within nodules in playa environments could be significantly influenced by burial processes. To elucidate the preservation of biosignatures in evaporitic lacustrine nodules, detailed examinations were conducted on carbonate nodules in the Qaidam Basin, which could be analogous to those found at Gale Crater on Mars in terms of the formation backgrounds and post-depositional processes. Microscopic and spectroscopic analyses revealed the presence of organic matter, including an organic annulus inferred to be a fossil spore or algal filament microfossil, within the Qaidam nodules. The TOC content of the Qaidam nodules was slightly higher than that of the surrounding fluvio-lacustrine deposits, suggesting that early cementation of carbonate matrix may be favorable for biomass preservation in playa diagenetic environments. The carbonate matrixes displayed alternating micritic and sparry layers characterized by radial-fibrous textures, along with enrichment of ^{13}C. These petrographic and geochemical characteristics suggested that the Qaidam nodules could be physicochemical precipitates though biomineralization and organomineralization cannot be excluded. The Raman spectral parameter I-1350/1,600 was indicative of changes in the structural order of carbonaceous materials, which could be sourced from carbon precursors of various subcellular components or coexisting organisms in pore waters. The $\delta^{13}C_{org}$ values provided evidence for carbon fixation pathways of the Calvin cycle or the Wood-Ljungdahl pathway metabolized by primary producers. This study demonstrated that terrestrial playa nodules provided a taphonomic window conducive to the preservation of organic biosignatures, with implications for the astrobiological significance of nodules at Gale Crater on Mars.

Data availability statement

The original contributions presented in the study are included in the article/Supplementary Material, further inquiries can be directed to the corresponding author.

Author contributions

YC: Conceptualization, Investigation, Formal Analysis, Methodology, Writing–original draft, Writing–review and editing. ZY: Supervision, Writing–review and editing, Funding acquisition. WL: Conceptualization, Project administration, Supervision, Funding acquisition, Writing–review and editing.

Funding

The author(s) declare that financial support was received for the research, authorship, and/or publication of this article. This research was supported by the National Key R&D Program of China (2022YFF0503204), National Natural Science Foundation of China (NSFC) grants (T2225011 and 42102341), the Key Research Program of the Chinese Academy of Sciences (ZDBS-SSW-TLC001), and CAS Interdisciplinary Innovation Team (JCTD-2020–18).

Acknowledgments

We thank Lixin Gu for his help with the SEM experiments and Xiaoguang Li for his help with the Raman experiments.

Conflict of interest

The authors declare that the research was conducted in the absence of any commercial or financial relationships that could be construed as a potential conflict of interest.

Publisher's note

Supplementary material

The Supplementary Material for this article can be found online at: https://www.frontiersin.org/articles/10.3389/fspas.2024.1291847/full#supplementary-material

References

Anglés, A., and Li, Y. (2017). The western Qaidam Basin as a potential Martian environmental analogue: an overview. *J. Geophys Res. Planets* 122 (5), 856–888. doi:10.1002/2017JE005293

Antunes, A., Lau Vetter, M. C. Y., Flannery, D., and Li, Y. (2023). Editorial: Mars analogs: environment, habitability and biodiversity. *Front. Astron Space Sci.* 10. doi:10.3389/fspas.2023.1208367

Arp, G., Wedemeyer, N., and Reitner, J. (2001). Fluvival tufa formation in a hard-water creek (deinschwanger bach, franconian Alb, Germany). *Facies* 44 (1), 1–22. doi:10.1007/BF02668163

Azua-Bustos, A., Fairén, A. G., González-Silva, C., Prieto-Ballesteros, O., Carrizo, D., Sánchez-García, L., et al. (2023). Dark microbiome and extremely low organics in Atacama fossil delta unveil Mars life detection limits. *Nat. Commun.* 14 (1), 808. doi:10.1038/s41467-023-36172-1

Balme, B. E. (1995). Fossil *in situ* spores and pollen grains: an annotated catalogue. *Rev. Palaeobot. Palyno* 87 (2), 81–323. doi:10.1016/0034-6667(95)93235-X

Beaty, D. W., Grady, M. M., Mcsween, H. Y., Sefton-Nash, E., Carrier, B. L., Altieri, F., et al. (2019). The potential science and engineering value of samples delivered to Earth by Mars sample return. *Meteorit. Planet. Sci.* 54 (S1), S3–S152. doi:10.1111/maps.13242

Beyssac, O., Goffé, B., Chopin, C., and Rouzaud, J. N. (2002). Raman spectra of carbonaceous material in metasediments: a new geothermometer. *J. Metamorph. Geol.* 20 (9), 859–871. doi:10.1046/j.1525-1314.2002.00408.x

Beyssac, O., Goffé, B., Petitet, J.-P., Froigneux, E., Moreau, M., and Rouzaud, J.-N. (2003). On the characterization of disordered and heterogeneous carbonaceous materials by Raman spectroscopy. *Spectrochimica Acta Part A Mol. Biomol. Spectrosc.* 59 (10), 2267–2276. doi:10.1016/S1386-1425(03)00070-2

Bishop, J. L. (2018). "Chapter 3 - remote detection of phyllosilicates on Mars and implications for climate and habitability," in *From habitability to life on Mars* Editors N. A. Cabrol, and E. A. Grin (Elsevier), 37–75.

Bonoldi, L., Di Paolo, L., and Flego, C. (2016). Vibrational spectroscopy assessment of kerogen maturity in organic-rich source rocks. *Vib. Spectrosc.* 87, 14–19. doi:10.1016/j.vibspec.2016.08.014

Bosak, T., Moore, K. R., Gong, J., and Grotzinger, J. P. (2021). Searching for biosignatures in sedimentary rocks from early Earth and Mars. *Nat. Rev. Earth Env.* 2, 490–506. doi:10.1038/s43017-021-00169-5

Buseck, P. R., and Beyssac, O. (2014). From organic matter to graphite: graphitization. *Elements* 10 (6), 421–426. doi:10.2113/gselements.10.6.421

Butterfield, N. J., Knoll, A. H., and Swett, K. (1990). A bangiophyte red alga from the Proterozoic of Arctic Canada. *Science* 250 (4977), 104–107. doi:10.1126/science.11538072

Chen, Q., Zhang, D., Wang, J., Zhao, F., Liu, Y., Zhang, Z., et al. (2020). Geochemical characteristics of carbonate rocks in a salinized lacustrine basin: a case study from Oligocene formation in the Qaidam Basin, northwestern China. *Carbonates Evaporites* 35 (2), 40. doi:10.1007/s13146-020-00551-2

Chen, Y., Diamond, C. W., Stüeken, E. E., Cai, C., Gill, B. C., Zhang, F., et al. (2019). Coupled evolution of nitrogen cycling and redoxcline dynamics on the Yangtze Block across the Ediacaran-Cambrian transition. *Geochimica Cosmochimica Acta* 257, 243–265. doi:10.1016/j.gca.2019.05.017

Chen, Y., Shen, J., Liu, L., Sun, Y., Pan, Y., and Lin, W. (2022). Preservation of organic matter in aqueous deposits and soils across the Mars-analog Qaidam Basin, NW China: implications for biosignature detection on Mars. *J. Geophys Res. Planets* 127 (12), e2022JE007418. doi:10.1029/2022JE007418

Chen, Y., Sun, Y., Liu, L., Shen, J., Qu, Y., Pan, Y., et al. (2023). Biosignatures preserved in carbonate nodules from the western Qaidam Basin, NW China: implications for life detection on Mars. *Astrobiology* 23 (2), 172–182. doi:10.1089/ast.2021.0196

Dupraz, C., Visscher, P. T., Baumgartner, L. K., and Reid, R. P. (2004). Microbe–mineral interactions: early carbonate precipitation in a hypersaline lake (Eleuthera Island, Bahamas). *Sedimentology* 51 (4), 745–765. doi:10.1111/j.1365-3091.2004.00649.x

Ehlmann, B. L., and Edwards, C. S. (2014). Mineralogy of the martian surface. *Annu. Rev. Earth Planet Sci.* 42 (1), 291–315. doi:10.1146/annurev-earth-060313-055024

Farley, K. A., Williford, K. H., Stack, K. M., Bhartia, R., Chen, A., De la Torre, M., et al. (2020). Mars 2020 mission overview. *Space Sci. Rev.* 216 (8), 142. doi:10.1007/s11214-020-00762-y

Foucher, F. (2019). "Detection of biosignatures using Raman spectroscopy," in *Biosignatures for Astrobiology* Editors B. Cavalazzi, and F. Westall (Cham: Springer International Publishing), 267–282.

Foucher, F., Ammar, M.-R., and Westall, F. (2015). Revealing the biotic origin of silicified Precambrian carbonaceous microstructures using Raman spectroscopic mapping, a potential method for the detection of microfossils on Mars. *J. Raman Spectrosc.* 46 (10), 873–879. doi:10.1002/jrs.4687

Franklin, R. E., and Randall, J. T. (1951). Crystallite growth in graphitizing and non-graphitizing carbons. *Proc. Math. Phys. Sci.* 209 (1097), 196–218. doi:10.1098/rspa.1951.0197

Freude, C., and Blaser, M. (2016). Carbon Isotope fractionation during catabolism and anabolism in acetogenic bacteria growing on different substrates. *Appl. Environ. Microbiol.* 82 (9), 2728–2737. doi:10.1128/AEM.03502-15

Gasda, P. J., Comellas, J., Essunfeld, A., Das, D., Bryk, A. B., Dehouck, E., et al. (2022). Overview of the morphology and chemistry of diagenetic features in the clay-rich Glen Torridon unit of Gale crater, Mars. *J. Geophys Res. Planets* 127, e2021JE007097. doi:10.1029/2021JE007097

Grice, K., Holman, A. I., Plet, C., and Tripp, M. (2019). Fossilised biomolecules and biomarkers in carbonate concretions from Konservat-Lagerstätten. *Minerals* 9 (3), 158. doi:10.3390/min9030158

Grotzinger, J., Sumner, D., Kah, L., Stack, K., Gupta, S., Edgar, L., et al. (2014). A habitable fluvio-lacustrine environment at yellowknife bay, Gale Crater, Mars. *Science* 343 (6169), 1242777. doi:10.1126/science.1242777

Grotzinger, J. P., Crisp, J., Vasavada, A. R., Anderson, R. C., Baker, C. J., Barry, R., et al. (2012). Mars Science Laboratory mission and science investigation. *Space Sci. Rev.* 170 (1), 5–56. doi:10.1007/s11214-012-9892-2

Grotzinger, J. P., and Rothman, D. H. (1996). An abiotic model for stromatolite morphogenesis. *Nature* 383 (6599), 423–425. doi:10.1038/383423a0

Haltigin, T., Hauber, E., Kminek, G., Meyer, M. A., Agee, C. B., Busemann, H., et al. (2022). Rationale and proposed design for a Mars sample return (MSR) science program. *Astrobiology* 22 (S1), S-27–S-56. doi:10.1089/ast.2021.0122

Han, W., Fang, X., Ye, C., Teng, X., and Zhang, T. (2014). Tibet forcing Quaternary stepwise enhancement of westerly jet and central Asian aridification: carbonate isotope records from deep drilling in the Qaidam salt playa, NE Tibet. *Glob. Planet Change* 116, 68–75. doi:10.1016/j.gloplacha.2014.02.006

Hays, L. E., Graham, H. V., Marais, D. J. D., Hausrath, E. M., Horgan, B., Mccollom, T. M., et al. (2017). Biosignature preservation and detection in Mars analog environments. *Astrobiology* 17 (4), 363–400. doi:10.1089/ast.2016.1627

Hügler, M., and Sievert, S. M. (2011). Beyond the Calvin cycle: autotrophic carbon fixation in the ocean. *Ann. Rev. Mar. Sci.* 3 (1), 261–289. doi:10.1146/annurev-marine-120709-142712

Hurley, S. J., Wing, B. A., Jasper, C. E., Hill, N. C., and Cameron, J. C. (2021). Carbon isotope evidence for the global physiology of Proterozoic cyanobacteria. *Sci. Adv.* 7 (2), eabc8998. doi:10.1126/sciadv.abc8998

Kano, A., Okumura, T., Takashima, C., and Shiraishi, F. (2019). "Cellular preservation in hydrated silicates that precipitate within modern carbonate microbialites," in *Geomicrobiological properties and processes of travertine: with a focus on Japanese sites* (Springer), 43–66.

Kminek, G., Meyer, M. A., Beaty, D. W., Carrier, B. L., Haltigin, T., and Hays, L. E. (2022). Mars sample return (MSR): planning for returned sample science. *Astrobiology* 22, S-1–S-4. doi:10.1089/ast.2021.0198

Knoll, A. H., Summons, R. E., Waldbauer, J. R., and Zumberge, J. E. (2007). "CHAPTER 8 - the geological succession of primary producers in the oceans," in *Evolution of primary producers in the sea* Editors P. G. Falkowski, and A. H. Knoll (Burlington: Academic Press), 133–163.

Kong, F., Zheng, M., Hu, B., Wang, A., Ma, N., and Sobron, P. (2018). Dalangtan saline playa in a hyperarid region on Tibet Plateau-I: evolution and environments. *Astrobiology* 18 (10), 1243–1253. doi:10.1089/ast.2018.1830

Kong, W. G., Zheng, M. P., Kong, F. J., and Chen, W. X. (2014). Sulfate-bearing deposits at Dalangtan Playa and their implication for the formation and preservation of martian salts†. *Am. Mineralogist* 99 (2-3), 283–290. doi:10.2138/am.2014.4594

Kouketsu, Y., Mizukami, T., Mori, H., Endo, S., Aoya, M., Hara, H., et al. (2014). A new approach to develop the Raman carbonaceous material geothermometer for low-grade metamorphism using peak width. *Isl. Arc* 23 (1), 33–50. doi:10.1111/iar.12057

Li, J., Dong, Z., Qian, G., Zhang, Z., Luo, W., Lu, J., et al. (2016a). Yardangs in the Qaidam Basin, northwestern China: distribution and morphology. *Aeolian Res.* 20, 89–99. doi:10.1016/j.aeolia.2015.11.002

Li, X., Chen, Y., Tang, X., Gu, L., Yuan, J., Su, W., et al. (2023). Thermally induced phase transition of troilite during micro-Raman spectroscopy analysis. *Icarus* 390, 115299. doi:10.1016/j.icarus.2022.115299

Li, X., Zhou, X., Liu, W., Wang, Z., He, Y., and Xu, L. (2016b). Carbon and oxygen isotopic records from Lake Tuosu over the last 120 years in the Qaidam Basin, Northwestern China: the implications for paleoenvironmental reconstruction. *Glob. Planet Change* 141, 54–62. doi:10.1016/j.gloplacha.2016.04.006

Liu, J., Li, C., Zhang, R., Rao, W., Cui, X., Geng, Y., et al. (2021). Geomorphic contexts and science focus of the Zhurong landing site on Mars. *Nat. Astron.* 6, 65–71. doi:10.1038/s41550-021-01519-5

Loyd, S. J., Meister, P., Liu, B., Nichols, K., Corsetti, F. A., Raiswell, R., et al. (2023). Temporal evolution of shallow marine diagenetic environments: insights from carbonate concretions. *Geochimica Cosmochimica Acta* 351, 152–166. doi:10.1016/j.gca.2023.04.022

Marshall, J. D., and Pirrie, D. (2013). Carbonate concretions—explained. *Geol. Today* 29 (2), 53–62. doi:10.1111/gto.12002

Mclennan, S. M., Anderson, R. B., Bell, J. F., Bridges, J. C., Calef, F., Campbell, J. L., et al. (2014). Elemental geochemistry of sedimentary rocks at Yellowknife bay, Gale crater, Mars. *Science* 343 (6169), 1244734. doi:10.1126/science.1244734

Mcmahon, S., Bosak, T., Grotzinger, J. P., Milliken, R. E., Summons, R. E., Daye, M., et al. (2018). A field guide to finding fossils on Mars. *J. Geophys Res. Planets* 123 (5), 1012–1040. doi:10.1029/2017JE005478

Meyer, M. A., Kminek, G., Beaty, D. W., Carrier, B. L., Haltigin, T., Hays, L. E., et al. (2022). Final report of the Mars sample return science planning group 2 (MSPG2). *Astrobiology* 22, S-5–S-26. 0 (ja), null. doi:10.1089/ast.2021.0121

Meyers, P. A., and Ishiwatari, R. (1993). "The early diagenesis of organic matter in lacustrine sediments," in *Organic geochemistry* Editors M. H. Engel, and S. A. Macko (Boston, MA: Springer), 185–209. doi:10.1007/978-1-4615-2890-6_8

Pedley, M. (1992). Freshwater (phytoherm) reefs: the role of biofilms and their bearing on marine reef cementation. *Sediment. Geol.* 79 (1), 255–274. doi:10.1016/0037-0738(92)90014-I

Plet, C., Grice, K., Scarlett, A. G., Ruebsam, W., Holman, A. I., and Schwark, L. (2020). Aromatic hydrocarbons provide new insight into carbonate concretion formation and the impact of eogenesis on organic matter. *Org. Geochem.* 143, 103961. doi:10.1016/j.orggeochem.2019.103961

Pratt, B. R. (1976) *Algal mats and cryptalgal structures, boca jewfish, lac, bonaire, Netherlands antilles*. Bachelor: McMaster University.

Rapin, W., Ehlmann, B. L., Dromart, G., Schieber, J., Thomas, N. H., Fischer, W. W., et al. (2019). An interval of high salinity in ancient Gale crater lake on Mars. *Nat. Geosci.* 12 (11), 889–895. doi:10.1038/s41561-019-0458-8

Saxena, R., Wijayawardene, N., Dai, D., Hyde, K., and Kirk, P. (2021). Diversity in fossil fungal spores. *Mycosphere* 12 (1), 670–874. doi:10.5943/mycosphere/12/1/8

Schidlowski, M. (1987). Application of stable carbon isotopes to early biochemical evolution on Earth. *Annu. Rev. Earth Planet. Sci.* 15 (1), 47–72. doi:10.1146/annurev.ea.15.050187.000403

Sforna, M. C., Van Zuilen, M. A., and Philippot, P. (2014). Structural characterization by Raman hyperspectral mapping of organic carbon in the 3.46 billion-year-old Apex chert, Western Australia. *Geochimica Cosmochimica Acta* 124, 18–33. doi:10.1016/j.gca.2013.09.031

Shen, J., Chen, Y., Sun, Y., Liu, L., Pan, Y., and Lin, W. (2022). Detection of biosignatures in terrestrial analogs of Martian regions: strategical and technical assessments. *Earth Planet Phys.* 6 (5), 431–450. doi:10.26464/epp2022042

Shkolyar, S., and Farmer, J. D. (2018). Biosignature preservation potential in playa evaporites: impacts of diagenesis and implications for Mars exploration. *Astrobiology* 18 (11), 1460–1478. doi:10.1089/ast.2018.1849

Simon, J., Hickman-Lewis, K., Cohen, B., Mayhew, L., Shuster, D., Vinciane, D., et al. (2023). Samples collected from the floor of Jezero crater with the Mars 2020 Perseverance rover. *J. Geophys Res. Planets* 128, e2022JE007474. doi:10.1029/2022JE007474

Snyder, R. G., Hsu, S. L., and Krimm, S. (1978). Vibrational spectra in the C-H stretching region and the structure of the polymethylene chain. *Spectrochim. Acta A Mol. Biomol. Spectrosc.* 34 (4), 395–406. doi:10.1016/0584-8539(78)80167-6

Stack, K. M., Grotzinger, J. P., Kah, L. C., Schmidt, M. E., Mangold, N., Edgett, K. S., et al. (2014). Diagenetic origin of nodules in the sheepbed member, yellowknife bay formation, Gale Crater, Mars. *J. Geophys Res. Planets* 119 (7), 1637–1664. doi:10.1002/2014JE004617

Summons, R. E., Amend, J. P., Bish, D., Buick, R., Cody, G. D., Marais, D. J. D., et al. (2011). Preservation of martian organic and environmental records: final report of the Mars biosignature working group. *Astrobiology* 11 (2), 157–181. doi:10.1089/ast.2010.0506

Sun, V., Stack, K., Kah, L., Thompson, L., Fischer, W., Williams, A., et al. (2018). Late-stage diagenetic concretions in the Murray formation, Gale crater, Mars. *Icarus* 321, 866–890. doi:10.1016/j.icarus.2018.12.030

Sun, Y., Li, Y., Li, K., Li, L., and He, H. (2021). Massive deposition of carbonate nodules in the hyperarid northwest Qaidam Basin of the northern Tibetan Plateau. *Geochem Geophy Geosy* 22, e2021GC009654. doi:10.1029/2021GC009654

Turner, E. C., and Jones, B. (2005). Microscopic calcite dendrites in cold-water tufa: implications for nucleation of micrite and cement. *Sedimentology* 52 (5), 1043–1066. doi:10.1111/j.1365-3091.2005.00741.x

Vaniman, D. T., Bish, D. L., Ming, D. W., Bristow, T. F., Morris, R. V., Blake, D. F., et al. (2014). Mineralogy of a mudstone at yellowknife bay, Gale Crater, Mars. *Science* 343 (6169), 1243480. doi:10.1126/science.1243480

Van Zuilen, M. A., Fliegel, D., Wirth, R., Lepland, A., Qu, Y., Schreiber, A., et al. (2012). Mineral-templated growth of natural graphite films. *Geochimica Cosmochimica Acta* 83, 252–262. doi:10.1016/j.gca.2011.12.030

Velthuis, M., Teurlincx, S., Van Dijk, G., Smolders, A. J. P., and De Senerpont domis, L. N. (2023). Salinisation effects on freshwater macrophyte growth and establishment in coastal eutrophic agricultural ditches. *Freshw. Biol.* 68 (4), 547–560. doi:10.1111/fwb.14046

Wagner, T., Magill, C. R., and Herrle, J. O. (2018). "Carbon isotopes," in *Encyclopedia of geochemistry: a comprehensive reference source on the chemistry of the Earth* Editor

W. M. White (Cham: Springer International Publishing), 194–204. doi:10.1007/978-3-319-39312-4_176

Ward, L. M., and Shih, P. M. (2019). The evolution and productivity of carbon fixation pathways in response to changes in oxygen concentration over geological time. *Free Radic. Biol. Med.* 140, 188–199. doi:10.1016/j.freeradbiomed.2019.01.049

Wiens, R. C., Rubin, D. M., Goetz, W., Fairén, A. G., Schwenzer, S. P., Johnson, J. R., et al. (2017). Centimeter to decimeter hollow concretions and voids in Gale crater sediments, Mars. *Icarus* 289, 144–156. doi:10.1016/j.icarus.2017.02.003

Xiao, L., Wang, J., Dang, Y., Cheng, Z., Huang, T., Zhao, J., et al. (2017). A new terrestrial analogue site for Mars research: the Qaidam Basin, Tibetan Plateau (NW China). *Earth Sci. Rev.* 164, 84–101. doi:10.1016/j.earscirev.2016.11.003

Xu, L., Li, H., Pei, Z., Zou, Y., and Wang, C. (2022). A brief introduction to the international Lunar research station program and the interstellar express mission. *Chin. J. Space Sci.* 42 (4), 511–513. doi:10.11728/cjss2022.04.yg28

Yan, N., Marschner, P., Cao, W., Zuo, C., and Qin, W. (2015). Influence of salinity and water content on soil microorganisms. *Int. Soil Water Conservation Res.* 3 (4), 316–323. doi:10.1016/j.iswcr.2015.11.003

Yang, H., Chen, Z.-Q., and Papineau, D. (2022). Cyanobacterial spheroids and other biosignatures from microdigitate stromatolites of mesoproterozoic wumishan formation in jixian, north China. *Precambrian Res.* 368, 106496. doi:10.1016/j.precamres.2021.106496

Yang, Z. (1986). "Cenozoic lithofacies paleogeography and its evolution in the Qaidam Basin," in *Late cenozoic geological environment evolution in the Qaidam Basin, qinghai province* (Beijing, China: Science Press).

Yin, A., Dang, Y., Wang, L., Jiang, W., Zhou, S., Chen, X., et al. (2008b). Cenozoic tectonic evolution of Qaidam basin and its surrounding regions (Part 1): the southern Qilian Shan-Nan Shan thrust belt and northern Qaidam basin. *Geol. Soc. Am. Bull.* 120 (7-8), 813–846. doi:10.1130/b26180.1

Yin, A., Dang, Y.-Q., Zhang, M., Chen, X.-H., and Mcrivette, M. W. (2008a). Cenozoic tectonic evolution of the Qaidam basin and its surrounding regions (Part 3): structural geology, sedimentation, and regional tectonic reconstruction. *Geol. Soc. Am. Bull.* 120 (7-8), 847–876. doi:10.1130/B26232.1

Zheng, X., Zhang, M., Xu, C., and Li, B. (2002) *Salt lakes of China*. Beijing: China Sci Press.